batteries

MDPI

Article

Low-Cost, Sustainable Hybrid Aqueous Zinc Metal Batteries Using Ethyl Cellulose as a Binder

Pedro Pablo Machado Pico, Stefano Colonna and Fabio Ronci *

Istituto di Struttura della Materia-CNR (ISM-CNR), Via del Fosso del Cavaliere 100, 00133 Roma, Italy; pedro.machado@artov.ism.cnr.it (P.P.M.P.); stefano.colonna@ism.cnr.it (S.C.)
* Correspondence: fabio.ronci@ism.cnr.it

Abstract: Despite their inherently lower energy density than lithium-ion batteries (LIBs), aqueous zinc metal batteries (AZMBs) have recently attracted interest as rechargeable energy storage devices due to their low cost and high operational and environmental safety. They are composed of metallic zinc as the anode, an aqueous zinc salt electrolyte and a cathode capable of (de)intercalating Zn^{2+} ions upon its (oxidation) reduction reaction. In this work, we studied a hybrid AZMB in which a dual-ion electrolyte containing both Zn^{2+} and Li^{+} ions was used in conjunction with a Li^{+} ion intercalation cathode, i.e., $LiFePO_4$ (LFP), one of the most common, reliable, and cheap cathodes for LIBs. In this study, we present evidence that, thanks to its insolubility in water, ethyl cellulose (EC) can be effectively utilized as a binder for cathode membranes in AZMBs. Furthermore, its solubility in alcohol provides a significant advantage in avoiding the use of toxic solvents, contributing to a safer and more environmentally friendly approach to the formulation process.

Keywords: aqueous zinc metal battery; lithium iron phosphate; ethyl cellulose; binder

check for updates

Academic Editor: Harry E. Hoster

Received: 27 February 2025
Revised: 5 May 2025
Accepted: 8 May 2025
Published: 11 May 2025

Citation: Machado Pico, P.P.; Colonna, S.; Ronci, F. Low-Cost, Sustainable Hybrid Aqueous Zinc Metal Batteries Using Ethyl Cellulose as a Binder. *Batteries* **2025**, *11*, 189. https://doi.org/10.3390/batteries11050189

Copyright: © 2025 by the authors. Licensee MDPI, Basel, Switzerland. This article is an open access article distributed under the terms and conditions of the Creative Commons Attribution (CC BY) license (https://creativecommons.org/licenses/by/4.0/).

1. Introduction

The development of energy storage systems for stationary applications is crucial for integrating renewable energy sources (solar, wind, etc.) into power grids. Batteries are recognized as a key element in the evolution of future electricity grids, enabling the decoupling of energy generation from consumption. Specifically, they are essential for integrating the inherently intermittent renewable energy sources into grids, providing grid support, frequency regulation, peak shaving, and enhancing the overall autonomy, reliability, stability, and cost-effectiveness of grids [1–6]. In this context, zinc ion batteries (ZIBs) are emerging as a promising alternative for next-generation energy storage devices, owing to their safety and low cost [7,8]. A typical aqueous zinc metal battery (AZMB) consists of metallic zinc as the anode, an aqueous electrolyte containing a zinc salt, and a cathode whose active material is typically a transition metal oxide that, similar to lithium-ion batteries (LIBs), can intercalate/deintercalate ions upon reduction/oxidation. The relatively low redox potential (−0.76 V vs. standard hydrogen electrode) enables the obtainment of devices with variable cell voltages from 0.8 to 2 V depending on the selected cathode material [9–11].

Common cathode materials in AZMBs include vanadium or manganese-based oxides [12–17], Prussian blue analogs (PBAs) [18–21], and organic-based materials [22–24] that can reversibly host Zn^{2+} ions within their crystalline structure. These materials often exhibit high specific capacity, in some cases approaching 300 $mAhg^{-1}$, combined with the high theorical capacity of the zinc metal anode (820 $mAhg^{-1}$), resulting in quite significant

specific energy values, close to 200 Wh Kg^{-1}, despite the low voltage associated with aqueous electrolytes [25,26].

A different approach is taken in hybrid AZMBs, where cathode materials typically used in LIBs, such as, e.g., $LiFePO_4$ (LFP) or $LiMn_2O_4$ (LMO), replace the aforementioned Zn-ion intercalation compounds. In this case, dual-ion electrolytes containing both Zn^{2+} and Li^+ ions are employed [27–29].

The cathode membrane is commonly prepared using the selected active material, a conductive additive (e.g., carbon black), and a polymeric binder. In LIBs, polyvinylidene fluoride (PVDF) is widely used as the binder of choice due to its electrochemical stability and strong adhesion to current collectors. However, the use of N-methyl-2-pyrrolidone (NMP), a hazardous and volatile organic solvent posing serious problems of safety and pollution [30,31], is necessary for the preparation of PVDF-based membranes. To address these issues, researchers have proposed the use of alternative nonfluorinated organic binders, such as carboxymethyl cellulose (CMC), cellulose acetate (CA), and sodium alginate (SA), which have lower environmental impact and costs [32–34].

Ethyl cellulose (EC) is a different cellulose derivative in which the cellulose hydroxyl -OH groups are partially replaced by ethoxy $-OCH_2CH_3$ groups, resulting in a decreased solubility in water with respect to CMC and CA, whose substituting groups are carboxymethyl $-CH_2COOH$ and acetoxy $-OC(=O)CH_3$ groups, respectively. On the other hand, EC is readily soluble in alcohol and has the qualities of being tasteless, colorless, and nontoxic [35]. Due to these properties, EC is utilized in protective coatings for pharmaceuticals and as additive for moisture protection and taste masking [36,37]. In the field of LIBs, EC has been successfully employed as a binder in non-aqueous systems [38,39].

In this work, we focused on the use of EC as the binder for the realization of cathode membranes based on LFP for aqueous ZMB batteries. The Zn||LFP system was evaluated using two different current collectors, i.e., AISI316 stainless steel (SS) and aluminum, and two different combinations of lithium sulfate (Li_2SO_4) and zinc sulfate ($ZnSO_4$) in dual-ion aqueous electrolyte. The results demonstrate that EC can be successfully used as a binder in hybrid zinc-ion aqueous battery systems.

2. Materials and Methods

2.1. Materials

Zn foil (purity > 99.9%, thickness 100 µm), AISI 316 stainless steel (10 µm), Al foil (>99.6%, 15 µm), $LiFePO_4$ (>99.99%), Super P carbon black and polyvinylidenefluoride (PVDF Solef 5130/1001) were purchased from MTI Corporation (Richmond, CA, USA). Ethyl cellulose (48.0–49.5% w/w ethoxyl basis) was purchased from Sigma-Aldrich (Saint Louis, MO, USA). Glass Microfiber Filters Whatman GF/A, lithium sulfate monohydrate ($Li_2SO_4 \cdot H_2O$, ≥99%), lithium acetate dihydrate ($LiAc \cdot 2H_2O$, ≥99.5%), zinc sulfate heptahydrate ($ZnSO_4 \cdot 7H_2O$, ≥99%), zinc acetate dihydrate ($Zn(Ac)_2$, ≥99.5%), 2-propanol (≥99.8%), and N-Methyl-2-pyrrolidone (NMP, 99%) were purchased from Carlo Erba (Cornaredo, Italy).

The electrolyte solutions were prepared by two different combinations of Li_2SO_4 and $ZnSO_4$ salts into Milli-Q H_2O (resistivity 18 MΩ·cm). The first one (1.5Li1.5Zn) was composed of Li_2SO_4 1.5 M + $ZnSO_4$ 1.5 M, the second one (3Li1.5Zn) of Li_2SO_4 3 M + $ZnSO_4$ 1.5 M.

The cathode membranes were prepared by mixing 200 mg of powder consisting of LFP (80 wt.%) as the active material, Super P (10 wt.%) as a conductive additive, and either EC or PVDF (10 wt.%) as the binder. The mixture was ground using a mortar for approximately 20 min. The resulting powder was then transferred to a small glass container, followed by the addition of 1 mL of isopropanol (for EC) or 1 mL of NMP (for PVDF) as the solvent. After stirring for 1 h at room temperature, the slurry was cast and evenly

distributed onto aluminum or stainless steel (SS) current collector foils using the doctor blade technique, with blade height set to 200 µm. Subsequently, the membranes were dried in an oven overnight at 70 °C or 110 °C (for EC and PVDF, respectively), cut into 10 mm diameter discs, and accurately weighed before use to determine the active material mass loading. On average, the active material mass loading of the electrodes used in this work was (1.3 ± 0.3) mg·cm^{-2}.

2.2. Methods

2.2.1. Electrochemical Characterization

Full Zn||LFP cells were assembled in Swagelok-type T-cells using a Whatman GF/A glass fiber separator soaked with the electrolyte. Galvanostatic charge–discharge (GCD) tests were performed at 0.1 Ag^{-1} (i.e., j~0.13 mAcm^{-2}).

SS (or Al) foil was used in asymmetric Zn||SS (or Zn||Al) cells as the working electrode in cyclic voltammetry (CV) tests for the initial study of the plating–stripping process (deposition–dissolution) of zinc and for the study of the electrochemical anodic stability window of the electrolyte.

GCD and CV tests were conducted using a multichannel battery cycler (Neware BTS-4000, Hong Kong, China) and a potentiostat/galvanostat (Metrohm Autolab PGSTAT302N, Herisau, Switzerland), respectively.

2.2.2. Morphological Characterization

The cathode membranes surface morphology was investigated using a scanning electron microscopy (SEM)–energy-dispersive X-ray spectroscopy (EDS) instrument (Thermo Fisher Scientific Phenom ProX Desktop, Waltham, MA, USA) at different magnification levels.

3. Results and Discussion

Two different EC-based membranes cast on Al and SS current collectors were initially tested in Zn||LFP full cells using two different electrolyte formulations, namely, 1.5Li1.5Zn and 3Li1.5Zn. GCD cycles performed at 0.1 Ag^{-1} between 0.7 and 1.7 V are reported in Figure 1, showing in all cases specific capacity values after 50 cycles ranging between about 110 and 130 mAhg^{-1}, with slightly better results observed when using the 3Li1.5Zn electrolyte (solid lines in Figure 1a).

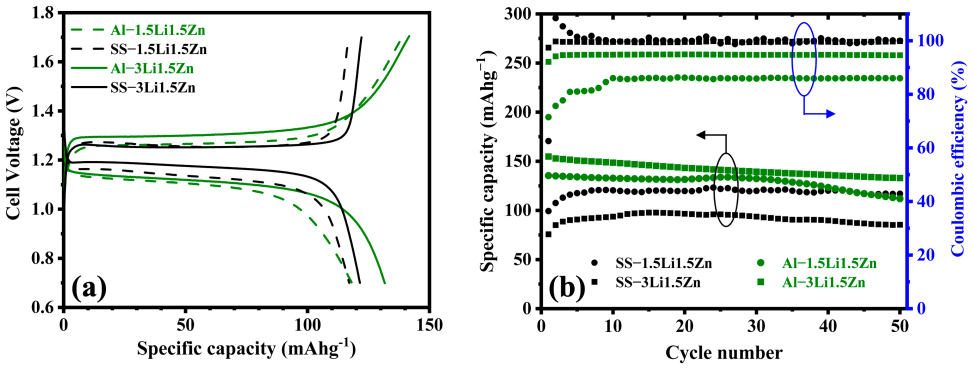


Figure 1. Cycling performance of Zn||LFP hybrid cells using LFP membranes with Al (green) or SS (black) current collectors and different aqueous electrolytes (3Li1.5Zn or 1.5Li1.5Zn). (**a**) Galvanostatic charge–discharge voltage profiles at the 50th cycle; (**b**) discharge's specific capacity and Coulombic efficiency.

Despite the higher specific capacity obtained by the 3Li1.5Zn electrolyte with Al current collectors, the better performance in terms of capacity retention and Coulombic efficiency was obtained by the membranes with SS current collectors (black symbols in

Figure 1b), which, after a few initial cycles, rapidly approached and maintained values close to 100% efficiency. On the contrary, the cycling performance of cells using Al as a current collector showed Coulombic efficiency values significantly below 100%.

This was an expected result since it is known that Al current collectors are prone to corrosion in neutral aqueous electrolyte solutions [40]. This was also confirmed by the clearly higher overpotential between the charge and discharge curves observed in Figure 1a when Al was used (green lines) rather than SS (black lines), due to the increased electrical resistance of the current collector caused by its corrosion.

CV tests were subsequently performed using two asymmetric cells: Zn||SS and Zn||Al to study the early stages of zinc deposition–dissolution (plating–stripping) and determine the electrochemical stability window of the 3Li1.5Zn electrolyte. The experiment consisted of three zinc plating–stripping cycles, followed by an anodic sweep until electrolyte decomposition was detected, as shown in Figure 2.

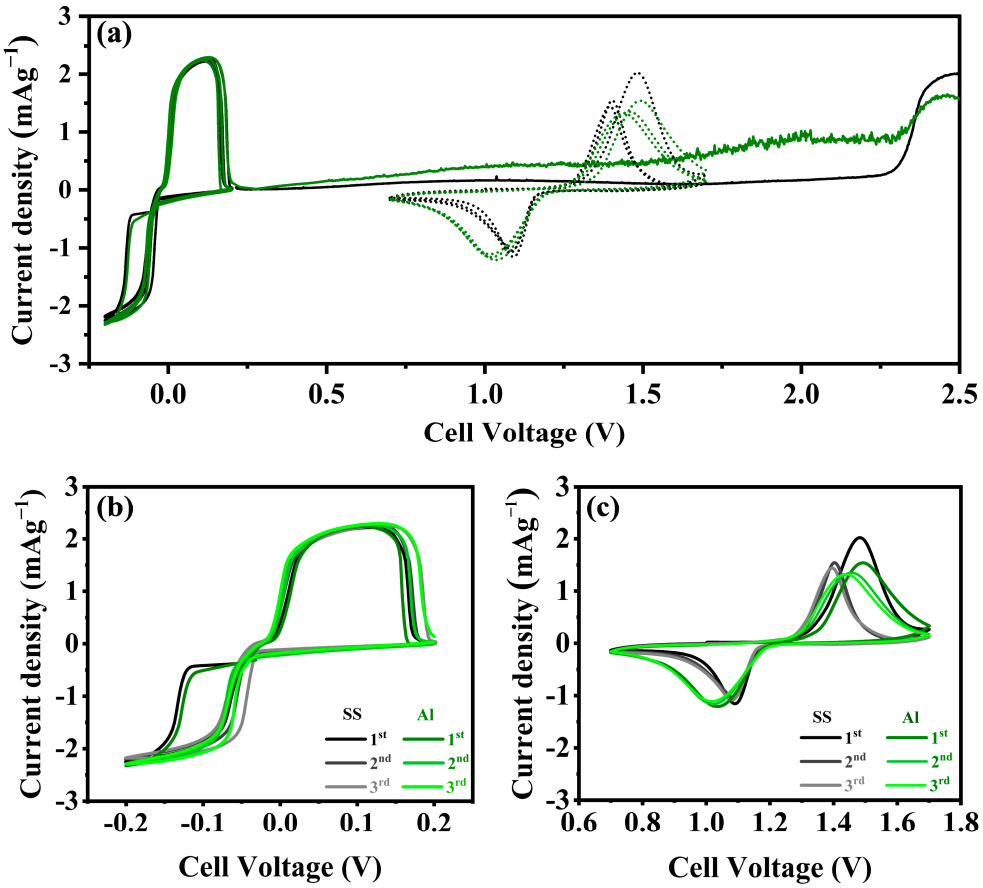


Figure 2. Electrochemical stability window of the 3Li1.5Zn electrolyte using SS (gray lines) and Al (green lines) foils as working electrode and Zn as the reference and counter electrodes: (**a**) CV (scan rate: 0.5 mVs^{-1}) consisting of three zinc plating–stripping cycles followed by an anodic sweep; (**b**) enlarged plot of the first 3 cycles of the Zn plating–stripping process in (**a**); (**c**) CVs of the first 3 cycles of a Zn||LFP cell highlighting the LFP activity window. The CVs are also reported as dotted lines in (**a**).

When SS was used as the current collector, the electrolyte demonstrated an anodic stability up to approximately 2.2 V, with current values very close to zero in the 0.7–1.7 V operating range of LFP (as evidenced by the CV curves of the electrode material in Figure 2c and superimposed in Figure 2a). Conversely, during the anodic sweep in the Zn||Al cell, the current already started to increase at very low voltage values, as shown by the quite

noisy green line. This evidence is ascribed to aluminum oxidation, which already starts to occur before 1 V, while electrolyte decomposition occurs near 2.2 V like for SS.

The leftmost region of the CV in Figure 2a is reported enlarged in the graph in Figure 2b, showing almost overlapping CV curves and similar anodic and cathodic peak areas during the first cycles, except for the first plating process occurring as expected at lower voltage, indicating the good reversibility of the plating–stripping process in both Zn-SS and Zn-Al cells.

Figure 2c reports the first three CV cycles of full cells assembled using a Zn anode, an LFP cathode coated on SS foil or Al foil, and the 3Li1.5Zn electrolyte. The anodic and cathodic peaks relative to the Li^+ ion deintercalation and intercalation in LFP were clearly observed to occur in the electrolyte stability window when SS was used as the current collector.

Before discarding the possibility to use the cheaper and lighter aluminum current collector, we verified the possible effect of the electrolyte anion on the aluminum corrosion by replacing the sulfate anion with the acetate anion.

Zn||LFP cells were assembled using a Zn foil as the anode and LFP membranes cast on aluminum as the cathode in 3Li1.5Zn electrolytes incorporating two different anions: sulfate and acetate. Figure 3a presents the GCD voltage profiles at the 50th cycle obtained in two-electrode cells with a 0.1 Ag^{-1} current density. Despite the higher specific capacity values recorded using the sulfate-based electrolyte, a lower Coulombic efficiency was clearly noted when comparing the charge and discharge's specific capacity values (132 and 141 $mAhg^{-1}$ for sulfate). On the other hand, the same value of 84 $mAhg^{-1}$ was obtained in both charge and discharge for the acetate-based electrolyte. This result was confirmed by the Coulombic efficiency data recorded upon cycling and reported in Figure 3b, showing an almost constant 94% value for sulfate and nearly 100% for acetate, suggesting that acetate mitigated the oxidation process of aluminum.

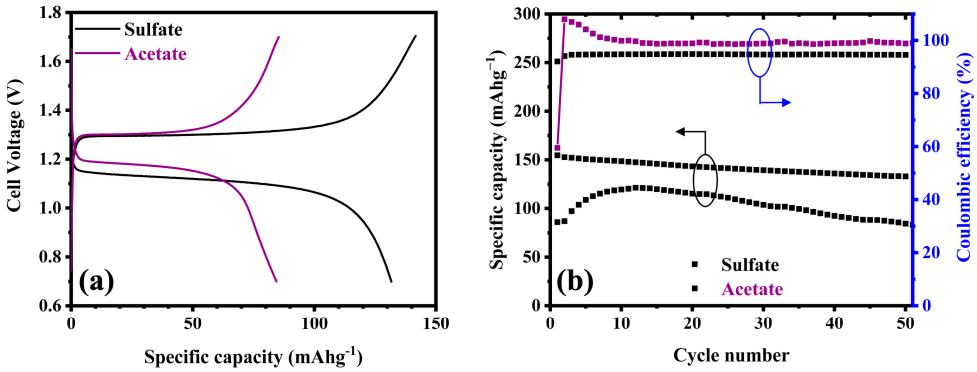


Figure 3. Cycling performance of Zn||LFP hybrid cells with an Al current collector using 3Li1.5Zn aqueous electrolytes with sulfate (black) and acetate (purple) anion. (**a**) Galvanostatic charge–discharge voltage profiles at the 50th cycle; (**b**) discharge's specific capacity and Coulombic efficiency.

Despite the better results in terms of specific capacity (see Figure 1), the performance of the cathode membranes with an aluminum current collector remained below expectations in terms of Coulombic efficiency. For this reason, we decided to proceed by using a standard SS current collector. To evaluate the quality of EC as a binder, we compared its properties with those of the conventional PVDF binder, producing LFP–Super-P–EC and LFP–Super-P–PVDF membranes in 8:1:1 weight ratio onto SS current collectors. We first compared the mechanical stability and morphology of the two types of membranes before their use. The results, reported in Figure 4, confirmed a similar resistance to membrane bending and twisting and comparable morphology in SEM images.

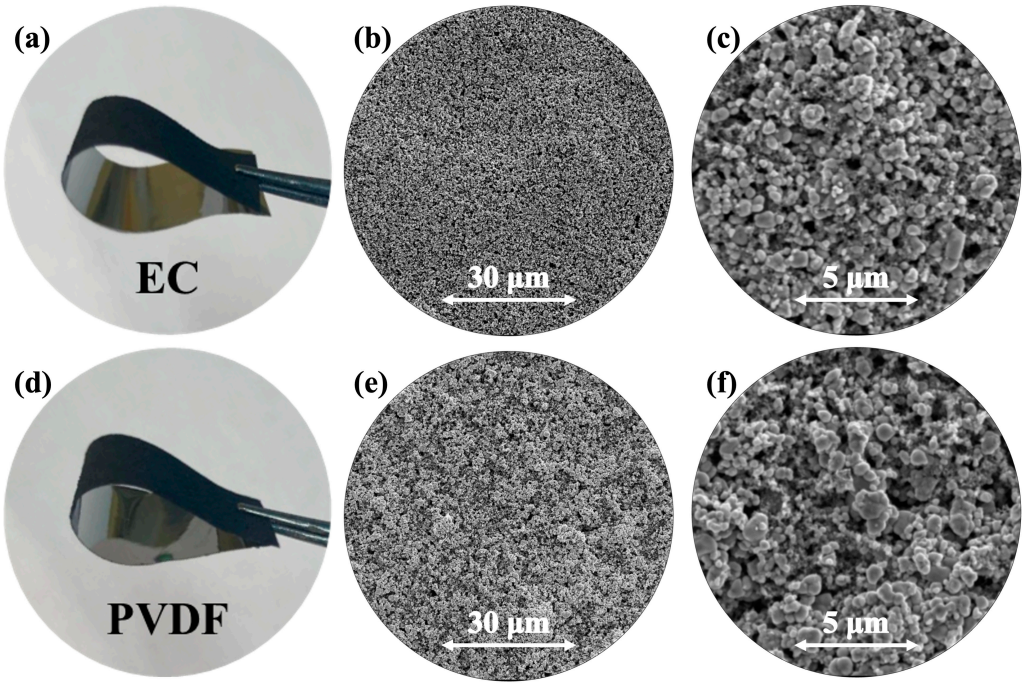


Figure 4. Image of bent membranes and SEM images at different magnifications of (**a**–**c**) EC-based and (**d**–**f**) PVDF-based membranes.

After verifying the mechanical stability and morphology, the two kinds of membranes were also compared for their electrochemical performance in full Zn||LFP cells using a 3Li1.5Zn sulfate electrolyte. In Figure 5, we report the results of 400-cycle GCD tests of EC- and PVDF-based LFP membranes performed at 0.2 Ag^{-1} in two-electrode cells.

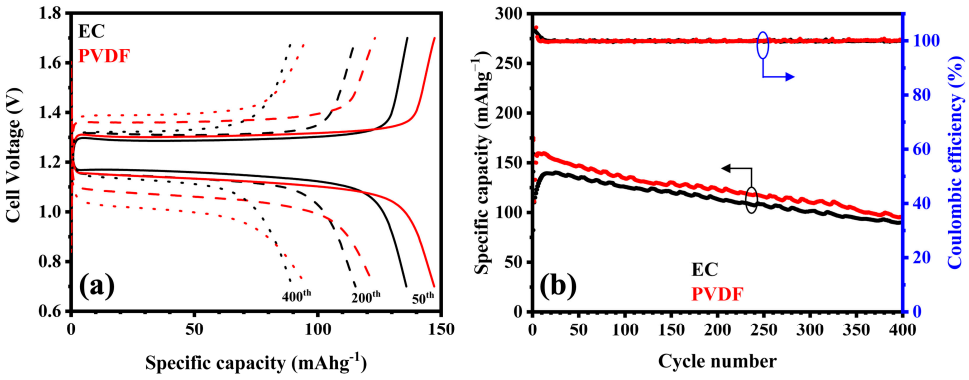


Figure 5. Cycling performance of Zn||LFP hybrid cells with EC (red) or PVDF (blue) binder using 3Li1.5Zn with sulfate anion. (**a**) GCD voltage profiles after 50, 200, and 400 cycles; (**b**) discharge's specific capacity and Coulombic efficiency.

The results showed that comparable performance was obtained with the two types of binders, as discussed below.

First of all, it must be noted that the small difference in specific capacity observed between the two curves in Figure 5b (approximately 10 $mAhg^{-1}$, <10%) was not significant, as it was smaller than the error associated with the active material mass obtained from the electrode weight procedure. Secondly, slightly better capacity retention was obtained using EC instead of PVDF (64% vs. 58% after 400 cycles), probably due to the lower overvoltage of EC-based electrodes at high cycle numbers; see Figure 5a.

This could be ascribed to the better wettability of cellulose-based binders with respect to PVDF [30]. To confirm this hypothesis, we performed static contact angle measurement

placing a 3Li1.5Zn electrolyte drop on both the EC- and the PVDF-based membranes and measuring the contact angle after 1 min. The results, reported in Figure 6, showed a lower contact angle for the EC-based membrane (115° vs. 133°), confirming the enhanced hydrophilicity of EC with respect to PVDF.

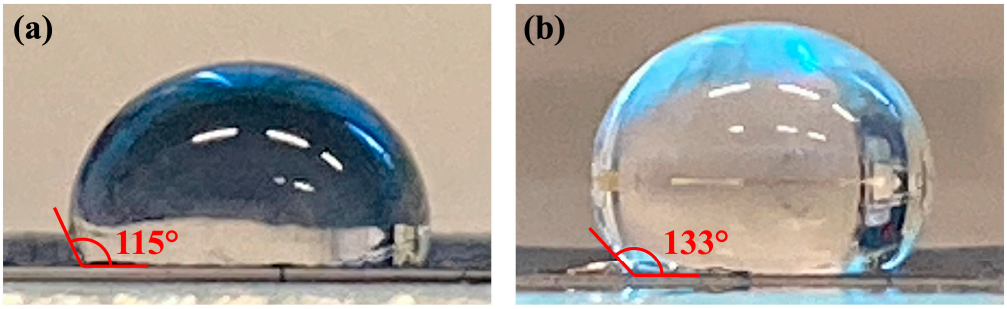


Figure 6. Static contact angle measurements of (**a**) the EC-based and (**b**) the PVDF-based membranes in contact with a drop of the 3Li1.5Zn electrolyte.

Interestingly, an increment in specific capacity values is observed in Figure 5b during the first cycles, reaching maximum values of about 140 $mAhg^{-1}$ and 160 $mAhg^{-1}$ after approximately 10 cycles using EC and PVDF as binder, respectively. This activation process was accompanied by Coulombic efficiency values higher than 100%, suggesting that partially irreversible phenomena occurred, using both kinds of electrodes, during the cell discharge process in the first cycles. This unexpected behavior, deserving a deeper study to be clearly understood, was similarly observed in a previous work [28] and could be tentatively attributed to the presence of both Zn^{2+} and Li^{+} ions in the dual-ion electrolyte, which could induce a partial, irreversible co-intercalation of Zn^{2+} ions in the LFP structure.

Figure 7 presents SEM images of the EC-based and PVDF-based LFP electrodes, measured before cycling and after 400 cycles. Negligible differences were observed between the pristine electrodes and the ones measured after 400 cycles in both electrodes. Higher magnification images revealed a possible small degree of LFP particle fracture, suggesting that cathode particle fragmentation could partly contribute to the observed capacity fade due to the reduced electrical connectivity of the active material particles.

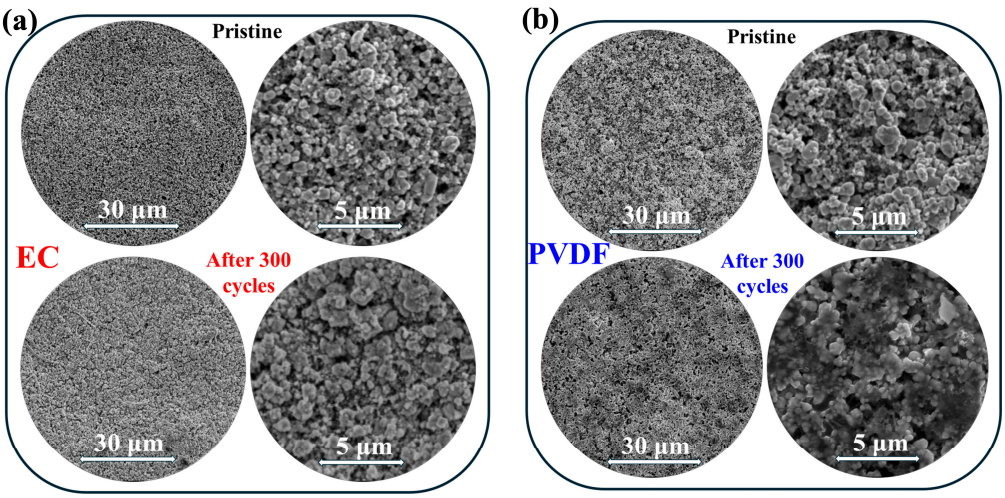


Figure 7. SEM images at different magnifications of (**a**) EC-based and (**b**) PVDF-based fresh membranes and after 400 GCD cycles.

An elemental analysis was also performed using energy-dispersive spectroscopy (EDS) mapping. The results, presented in Figure 8a (EC) and Figure 8b (PVDF), showed

a uniformly distributed mapping of the main elements (C, O, Fe, and P for EC and C, O, Fe, P, and F for PVDF) in both cases before cycling. The main elements' distribution of the two types of membranes after 400 GCD cycles in Figure 5 remained equally uniform and showed the additional presence of Zn and S elements due to residual electrolyte and/or electrolyte decomposition products.

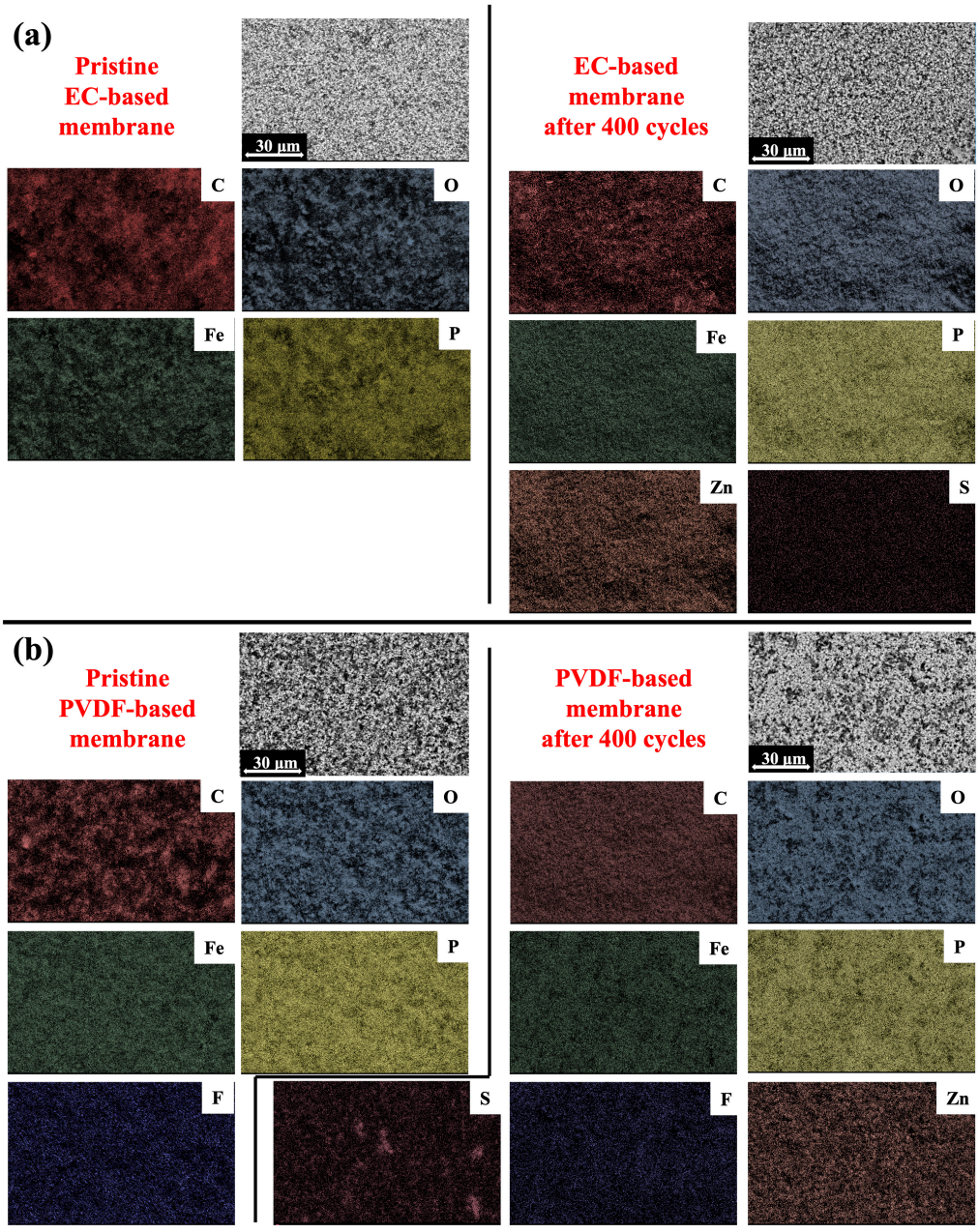


Figure 8. EDS element mapping images of LFP membranes using EC (**a**) and PVDF (**b**) as binder.

4. Conclusions

In this study, we explored the potential use of ethyl cellulose as a binder for the fabrication of cathode membranes for use in aqueous zinc metal batteries. We tested EC-based membranes using LFP as the active material in hybrid Zn||LFP batteries, utilizing different dual-ion electrolyte formulations with zinc–lithium sulfate–acetate salts, and different current collectors, Al and SS. The results indicated better results using dual-ion sulfate-based electrolytes and an SS current collector.

The mechanical properties, composition, and electrochemical performance of the EC-based membranes were compared to analogous PVDF-based membranes, demonstrating that similar results could be achieved using EC instead of PVDF as a binder, eliminating the need for the toxic and costly NMP solvent. This approach further enhances the already high sustainability of aqueous zinc metal batteries in terms of cost, safety, and environmental impact.

Author Contributions: Conceptualization, P.P.M.P. and F.R.; methodology, P.P.M.P. and F.R.; validation, P.P.M.P., S.C., and F.R.; formal analysis, P.P.M.P., S.C., and F.R.; investigation, P.P.M.P. and F.R.; resources, F.R.; data curation, P.P.M.P. and F.R.; writing—original draft preparation, P.P.M.P. and F.R.; writing—review and editing, F.R. and S.C.; supervision, F.R.; project administration, F.R.; funding acquisition, F.R. All authors have read and agreed to the published version of the manuscript.

Funding: This work was supported by the IEMAP (Italian Energy Materials Acceleration Platform) project funded by MASE (formerly MiTE) Ministry under the international Mission Innovation initiative.

Data Availability Statement: The original contributions presented in the study are included in the article. Further inquiries can be directed to the corresponding author.

Acknowledgments: The authors acknowledge the valuable technical support of Giovanni Emma, and Marco Ortenzi.

Conflicts of Interest: The authors declare no conflicts of interest.

References

1. Koholé, Y.W.; Wankouo Ngouleu, C.A.; Fohagui, F.C.V.; Tchuen, G. A Comprehensive Comparison of Battery, Hydrogen, Pumped-Hydro and Thermal Energy Storage Technologies for Hybrid Renewable Energy Systems Integration. *J. Energy Storage* **2024**, *93*, 112299. [CrossRef]
2. Sun, H.; Xiang, X.; Wang, X.; Tsai, H.S.; Feng, W. Advanced Photo-Rechargeable Lithium- and Zinc-Ion Batteries: Progress and Prospect. *J. Power Sources* **2024**, *598*, 234204. [CrossRef]
3. Adeyinka, A.M.; Esan, O.C.; Ijaola, A.O.; Farayibi, P.K. Advancements in Hybrid Energy Storage Systems for Enhancing Renewable Energy-to-Grid Integration. *Sustain. Energy Res.* **2024**, *11*, 26. [CrossRef]
4. Abo-Khalil, A.G.; Alobaid, M. A Guide to the Integration and Utilization of Energy Storage Systems with a Focus on Demand Resource Management and Power Quality Enhancement. *Sustainability* **2023**, *15*, 14680. [CrossRef]
5. Bullich-Massagué, E.; Cifuentes-García, F.-J.; Glenny-Crende, I.; Cheah-Mañé, M.; Aragüés-Peñalba, M.; Díaz-González, F.; Gomis-Bellmunt, O. A Review of Energy Storage Technologies for Large Scale Photovoltaic Power Plants. *Appl. Energy* **2020**, *274*, 115213. [CrossRef]
6. Zhang, Z.; Ding, T.; Zhou, Q.; Sun, Y.; Qu, M.; Zeng, Z.; Ju, Y.; Li, L.; Wang, K.; Chi, F. A Review of Technologies and Applications on Versatile Energy Storage Systems. *Renew. Sustain. Energy Rev.* **2021**, *148*, 111263. [CrossRef]
7. Ho, V.C.; Lim, H.; Kim, M.J.; Mun, J. Improving the Performance of Aqueous Zinc-Ion Batteries by Inhibiting Zinc Dendrite Growth: Recent Progress. *Chem. Asian J.* **2022**, *17*, e202200289. [CrossRef]
8. Han, J.; Euchner, H.; Kuenzel, M.; Hosseini, S.M.; Groß, A.; Varzi, A.; Passerini, S. A Thin and Uniform Fluoride-Based Artificial Interphase for the Zinc Metal Anode Enabling Reversible Zn/MnO_2 Batteries. *ACS Energy Lett.* **2021**, *6*, 3063–3071. [CrossRef]
9. Wang, J.; Wang, J.G.; Liu, H.; You, Z.; Wei, C.; Kang, F. Electrochemical Activation of Commercial MnO Microsized Particles for High-Performance Aqueous Zinc-Ion Batteries. *J. Power Sources* **2019**, *438*, 226951. [CrossRef]
10. Li, H.; Ma, L.; Han, C.; Wang, Z.; Liu, Z.; Tang, Z.; Zhi, C. Advanced Rechargeable Zinc-Based Batteries: Recent Progress and Future Perspectives. *Nano Energy* **2019**, *62*, 550–587. [CrossRef]
11. Liu, H.; Wang, J.G.; You, Z.; Wei, C.; Kang, F.; Wei, B. Rechargeable Aqueous Zinc-Ion Batteries: Mechanism, Design Strategies and Future Perspectives. *Mater. Today* **2021**, *42*, 73–98. [CrossRef]
12. Wu, B.; Li, M.; Mazánek, V.; Liao, Z.; Ying, Y.; Oliveira, F.M.; Dekanovsky, L.; Jan, L.; Hou, G.; Antonatos, N.; et al. In Situ Vanadium-Deficient Engineering of V2C MXene: A Pathway to Enhanced Zinc-Ion Batteries. *Small Methods* **2024**, *8*, e2301461. [CrossRef]
13. Chen, X.; Zhang, H.; Liu, J.H.; Gao, Y.; Cao, X.; Zhan, C.; Wang, Y.; Wang, S.; Chou, S.L.; Dou, S.X.; et al. Vanadium-Based Cathodes for Aqueous Zinc-Ion Batteries: Mechanism, Design Strategies and Challenges. *Energy Storage Mater.* **2022**, *50*, 21–46. [CrossRef]

14. Li, S.; Qin, L.; Li, L.; Cheng, H.; Fang, G.; Liang, S.; Zhu, Q.; Chen, M. Porous Structure ZnV_2O_4/C-N Composite Activating Vanadium-Based Cathode in Aqueous Zinc-Ion Batteries. *Mater. Today Commun.* **2021**, *27*, 102271. [CrossRef]
15. Li, Q.; Ye, X.; Yu, H.; Du, C.; Sun, W.; Liu, W.; Pan, H.; Rui, X. Pre-Potassiated Hydrated Vanadium Oxide as Cathode for Quasi-Solid-State Zinc-Ion Battery. *Chin. Chem. Lett.* **2022**, *33*, 2663–2668. [CrossRef]
16. Mathew, V.; Sambandam, B.; Kim, S.; Kim, S.; Park, S.; Lee, S.; Alfaruqi, M.H.; Soundharrajan, V.; Islam, S.; Putro, D.Y.; et al. Manganese and Vanadium Oxide Cathodes for Aqueous Rechargeable Zinc-Ion Batteries: A Focused View on Performance, Mechanism, and Developments. *ACS Energy Lett.* **2020**, *5*, 2376–2400. [CrossRef]
17. Han, M.; Qin, L.; Liu, Z.; Zhang, L.; Li, X.; Lu, B.; Huang, J.; Liang, S.; Zhou, J. Reaction Mechanisms and Optimization Strategies of Manganese-Based Materials for Aqueous Zinc Batteries. *Mater. Today Energy* **2021**, *20*, 100626. [CrossRef]
18. Syed, W.A.; Kakarla, A.K.; Bandi, H.; Shanthappa, R.; Yu, J.S. Copper Substituted Manganese Prussian Blue Analogue Composite Nanostructures for Efficient Aqueous Zinc-Ion Batteries. *J. Energy Storage* **2024**, *99*, 113325. [CrossRef]
19. Li, Y.; Zhao, J.; Hu, Q.; Hao, T.; Cao, H.; Huang, X.; Liu, Y.; Zhang, Y.; Lin, D.; Tang, Y.; et al. Prussian Blue Analogs Cathodes for Aqueous Zinc Ion Batteries. *Mater. Today Energy* **2022**, *29*, 101095. [CrossRef]
20. Li, M.; Maisuradze, M.; Sciacca, R.; Hasa, I.; Giorgetti, M. A Structural Perspective on Prussian Blue Analogues for Aqueous Zinc-Ion Batteries. *Batter. Supercaps* **2023**, *6*, e202300340. [CrossRef]
21. Liu, J.; Shen, Z.; Lu, C.Z. Research Progress of Prussian Blue and Its Analogues for Cathodes of Aqueous Zinc Ion Batteries. *J. Mater. Chem. A Mater.* **2024**, *12*, 2647–2672. [CrossRef]
22. Li, C.; Hu, L.; Ren, X.; Lin, L.; Zhan, C.; Weng, Q.; Sun, X.; Yu, X. Asymmetric Charge Distribution of Active Centers in Small Molecule Quinone Cathode Boosts High-Energy and High-Rate Aqueous Zinc-Organic Batteries. *Adv. Funct. Mater.* **2024**, *34*, 2313241. [CrossRef]
23. Dey, G.; Fayaz, A.; Jasmin, R.M.; Dinesan, S.; Sampath, S. A Copolymer of Benzoquinone and Pyrrole as High Rate, Durable Polymer Electrode for Aqueous Zn- and Mg-Ion Based Batteries. *Chem. Asian J.* **2025**, *20*, e202401135. [CrossRef]
24. Song, Z.; Huang, Q.; Lv, Y.; Gan, L.; Liu, M. Multi-N-Heterocycle Donor-Acceptor Conjugated Amphoteric Organic Superstructures for Superior Zinc Batteries. *Angew. Chem.—Int. Ed.* **2024**, *64*, e202418237. [CrossRef] [PubMed]
25. Zeng, X.; Hao, J.; Wang, Z.; Mao, J.; Guo, Z. Recent Progress and Perspectives on Aqueous Zn-Based Rechargeable Batteries with Mild Aqueous Electrolytes. *Energy Storage Mater.* **2019**, *20*, 410–437. [CrossRef]
26. Innocenti, A.; Bresser, D.; Garche, J.; Passerini, S. A Critical Discussion of the Current Availability of Lithium and Zinc for Use in Batteries. *Nat. Commun.* **2024**, *15*, 4068. [CrossRef] [PubMed]
27. Han, J.; Mariani, A.; Varzi, A.; Passerini, S. Green and Low-Cost Acetate-Based Electrolytes for the Highly Reversible Zinc Anode. *J. Power Sources* **2021**, *485*, 229329. [CrossRef]
28. Zhong, X.; Wang, F.; Ding, Y.; Duan, L.; Shi, F.; Wang, C. Water-in-Salt Electrolyte Zn/$LiFePO_4$ Batteries. *J. Electroanal. Chem.* **2020**, *867*, 114193. [CrossRef]
29. Zhao, J.; Li, Y.; Peng, X.; Dong, S.; Ma, J.; Cui, G.; Chen, L. High-Voltage Zn/$LiMn_{0.8}Fe_{0.2}PO_4$ Aqueous Rechargeable Battery by Virtue of "Water-in-Salt" Electrolyte. *Electrochem. Commun.* **2016**, *69*, 6–10. [CrossRef]
30. Zhang, X.; Ge, X.; Shen, Z.; Ma, H.; Wang, J.; Wang, S.; Liu, L.; Liu, B.; Liu, L.; Zhao, Y. Green Water-Based Binders for $LiFePO_4$/C Cathodes in Li-Ion Batteries: A Comparative Study. *New J. Chem.* **2021**, *45*, 9846–9855. [CrossRef]
31. Prosini, P.P.; Carewska, M.; Cento, C.; Masci, A. Poly Vinyl Acetate Used as a Binder for the Fabrication of a $LiFePO_4$-Based Composite Cathode for Lithium-Ion Batteries. *Electrochim. Acta* **2014**, *150*, 129–135. [CrossRef]
32. Bresser, D.; Buchholz, D.; Moretti, A.; Varzi, A.; Passerini, S. Alternative Binders for Sustainable Electrochemical Energy Storage-the Transition to Aqueous Electrode Processing and Bio-Derived Polymers. *Energy Environ. Sci.* **2018**, *11*, 3096–3127. [CrossRef]
33. Islam, S.; Alfaruqi, M.H.; Mathew, V.; Song, J.; Kim, S.; Kim, S.; Jo, J.; Baboo, J.P.; Pham, D.T.; Putro, D.Y.; et al. Facile Synthesis and the Exploration of the Zinc Storage Mechanism of β-MnO_2 Nanorods with Exposed (101) Planes as a Novel Cathode Material for High Performance Eco-Friendly Zinc-Ion Batteries. *J. Mater. Chem. A Mater.* **2017**, *5*, 23299–23309. [CrossRef]
34. Ding, Y.; Zhong, X.; Yuan, C.; Duan, L.; Zhang, L.; Wang, Z.; Wang, C.; Shi, F. Sodium Alginate Binders for Bivalency Aqueous Batteries. *ACS Appl. Mater. Interfaces* **2021**, *13*, 20681–20688. [CrossRef] [PubMed]
35. Kapoor, D.; Maheshwari, R.; Verma, K.; Sharma, S.; Ghode, P.; Tekade, R.K. *Coating Technologies in Pharmaceutical Product Development*; Elsevier Inc.: Amsterdam, The Netherlands, 2020; ISBN 9780128144879.
36. Riaz, A.; Abdul-wahhab, A.; Irfan, M. *Aqueous Polymeric Coatings: New Opportunities in Drug Delivery Systems*; Elsevier Inc.: Amsterdam, The Netherlands, 2020; ISBN 9780128212226.
37. Wasilewska, K.; Winnicka, K. Ethylcellulose-a Pharmaceutical Excipient with Multidirectional Application in Drug Dosage Forms Development. *Materials* **2019**, *12*, 3386. [CrossRef]
38. Zhang, J.; Zhong, H.; Zheng, C.; Xia, Y.; Liang, C.; Huang, H.; Gan, Y.; Tao, X.; Zhang, W. All-solid-state batteries with slurry coated $LiNi_{0.8}Co_{0.1}Mn_{0.1}O_2$ composite cathode and Li_6PS_5Cl electrolyte: Effect of binder content. *J. Power Sources* **2018**, *391*, 73–79. [CrossRef]

39. Zuo, X.; Ma, X.; Wu, J.; Deng, X.; Xiao, X.; Liu, J.; Nan, J. Self-supporting ethyl cellulose/poly(vinylidene fluoride) blended gel polymer electrolyte for 5 V high-voltage lithium-ion batteries. *Electrochim. Acta* **2018**, *271*, 582–590. [CrossRef]
40. Zhang, H.; Liu, X.; Li, H.; Hasa, I.; Passerini, S. Challenges and Strategies for High-Energy Aqueous Electrolyte Rechargeable Batteries. *Angew. Chem.—Int. Ed.* **2021**, *60*, 598–616. [CrossRef]

Disclaimer/Publisher's Note: The statements, opinions and data contained in all publications are solely those of the individual author(s) and contributor(s) and not of MDPI and/or the editor(s). MDPI and/or the editor(s) disclaim responsibility for any injury to people or property resulting from any ideas, methods, instructions or products referred to in the content.